

# Reduced order modelling method via proper orthogonal decomposition (POD) for flow around an oscillating cylinder

E. Liberge\*, A. Hamdouni

*LEPTIAB Université de la Rochelle, Avenue Michel Crépeau, 17042 La Rochelle Cedex 1, France*

Received 8 April 2008; accepted 6 October 2008

Available online 25 January 2010

---

## Abstract

This paper presents reduced order modelling (ROM) in fluid–structure interaction (FSI). The ROM via the proper orthogonal decomposition (POD) method has been chosen, due to its efficiency in the domain of fluid mechanics. POD-ROM is based on a low-order dynamical system obtained by projecting the nonlinear Navier–Stokes equations on a smaller number of POD modes. These POD modes are spatial and temporally independent. In FSI, the fluid and structure domains are moving, owing to which the POD method cannot be applied directly to reduce the equations of each domain. This article proposes to compute the POD modes for a global velocity field (fluid and solid), and then to construct a low-order dynamical system. The structure domain can be decomposed as a rigid domain, with a finite number of degrees of freedom. This low-order dynamical system is obtained by using a multiphase method similar to the fictitious domain method. This multiphase method extends the Navier–Stokes equations to the solid domain by using a penalisation method and a Lagrangian multiplier. By projecting these equations on the POD modes obtained for the global velocity field, a nonlinear low-order dynamical system is obtained and tested on a case of high Reynolds number.

© 2009 Elsevier Ltd. All rights reserved.

*Keywords:* Reduced order modelling (ROM); Proper orthogonal decomposition (POD); Low-order dynamical system; Fluid–structure interaction

---

## 1. Introduction

Computational modelling of fluid–structure interaction has remained a challenging area of research over the past few decades. Many efficient methodologies and algorithms to model FSI have evolved in the recent past. The computational cost associated with these models can be an important limiting factor. For example, in case of active control, where computation in quasi-real time is required, FSI models are not adapted. In the shape optimisation domain, changing one parameter leads to recomputing the entire model, which can be time consuming.

In the present paper, we study reduced order modelling (ROM) in these contexts. The ROM based on a projection of the problem's equations onto a basis obtained by a first computation is considered, but this makes the building of ROM quite expensive. The main objective is to use the constructed ROM in shape optimisation for a set of parameters different from those used to build them, or, in another example, for a longer time period than the first computation.

---

\*Corresponding author.

*E-mail address:* [eliberge@univ-lr.fr](mailto:eliberge@univ-lr.fr) (E. Liberge).

It would also be interesting for coupled problems if the reduced model which has been constructed for the phenomena which have a larger time scale is solved with the smaller time scale. Another example deals with active control or stability study.

ROM applied to FSI has emerged as an area of interest very recently. Different methods have been proposed for the analysis of FSI; the most significant are discussed by Dowell and Hall (2001).

There are two possible ways to construct ROM. The most famous uses the notion of eigenmodes of the fluid flow. This approach characterises a field in terms of a relatively small number of global modes. Under the term “mode” a distribution of variables that characterises a gross motion of the studied physical system is understood. There are several techniques to find these modes. One of these techniques concentrates on extracting the eigenmodes from the used model (Romanowski and Dowell, 1996), a finite element model for example. However, in case of a very large-dimensional system, extracting eigenmodes can be computationally very expensive. Thus, we use another method, such as the method of balanced modes (Baker et al., 1996) or the proper orthogonal decomposition (POD) which will be explained in detail in Section 2. The second technique to determine ROM is the input/output model. This method uses a transfer function that typically receives input in structure modes and gives the generalised forces weighted by structural modes (Karpel, 1982) as output.

The intention of the present study is to explore the capabilities of POD in FSI. This method was introduced by Lumley (1967) in fluid mechanics in order to extract coherent structures in a turbulent fluid flow. It has been intensively used since the 1990s in many applications, such as flows in a driven cavity (Cazemier et al., 1998), in boundary layer flows (Sirovich et al., 1990), or in particle dispersion (Allery et al., 2005).

In structural mechanics, POD is a domain of interest similar to modal analysis (Amabili and Touze, 2007; Amabili et al., 2006; Trindade et al., 2005) in case of structural vibration. There are very few studies available in fluid–structure interaction; an overview of the most significant ones are presented in Section 3.

First, this paper recalls the well-known POD method and its application in fluid mechanics. Then, it explains the constraint of applying POD in the FSI domain and also proposes a solution to build low-order dynamical systems. Last, the method proposed is applied for a typical case of FSI with a rigid solid domain.

## 2. The proper orthogonal decomposition (POD)

### 2.1. The POD formulation

In this section, the POD method is briefly introduced, following the formulations of Lumley (1967) and Sirovich (1987). A detailed methodology has already been proposed in the literature (Lumley, 1967; Holmes et al., 1998; Allery, 2002; Berkooz et al., 1993).

Consider a space  $\Omega \subset \mathbb{R}^d$ ,  $d = 1, 2$  or  $3$ ,  $(O, \mathbf{x}_1, \mathbf{x}_2, \mathbf{x}_3)$  a reference datum tied to this space,  $\mathbf{T} \subset \mathbb{R}$ ,  $x \in \Omega$ ,  $t \in \mathbf{T}$ . The POD consists in finding a deterministic function  $\psi$ , in a Hilbert space  $\mathbf{H}$ , which gives the optimum representation of a velocity field  $v(x, t) \in \mathbf{H}(\Omega, \mathbf{T})$ ,<sup>1</sup> by solving the following maximisation problem:

$$\max_{\psi \in \mathbf{H}} \frac{\langle (v, \psi)^2 \rangle}{(\psi, \psi)} = \frac{\langle (v, \Phi)^2 \rangle}{(\Phi, \Phi)}, \quad (1)$$

where  $\langle \bullet \rangle$  denotes a statistically average operator,  $(\bullet, \bullet)$  denotes the inner product of  $\mathbf{H}$  and  $\|\bullet\|_{\mathbf{H}}$  the associated norm. In the case of  $\mathbf{H} = \mathbf{L}^2(\Omega)$ , the maximisation of problem (1) leads to solving the following eigenvalue problem:

$$\int_{\Omega} \mathcal{R}(x, x') \Phi(x') dx' = \lambda \Phi(x), \quad (2)$$

where  $\mathcal{R}$  is the symmetric spatial correlation tensor, defined non-negative:

$$\mathcal{R}(x, x') = \langle v(\bullet, x) \otimes v(\bullet, x') \rangle. \quad (3)$$

Moreover, if  $\mathcal{R}$  is continuous, the following operator

$$\mathcal{R} : \mathbf{H} \rightarrow \mathbf{H}, \quad (4)$$

$$\Phi \mapsto \int_{\Omega} \mathcal{R}(x, x') \Phi(x') dx', \quad (5)$$

<sup>1</sup> $v$  can also be a vector whose the components are the pressure, the density, the vorticity, etc.

is compact. Then the Hilbert–Schmidt theorem assures that there exists a set of positive eigenvalues  $(\lambda_i)_{i \geq 1}$  which decreases to 0,

$$\lambda_1 > \lambda_2 > \dots > \lambda_i > \dots \quad \text{and} \quad \lambda_i \rightarrow 0, \quad (6)$$

and a set of eigenmodes  $(\Phi_i)_{i \geq 1}$  which is a Hilbert basis for  $\mathbf{H}$ . Thus,  $v$  can be decomposed according to the eigenmodes as

$$v(x, t) = \sum_{i=1}^{\infty} a_i(t) \Phi_i(x) \quad \text{in } \mathbf{L}^2(\Omega) \text{ sense,} \quad (7)$$

where  $a_i$  are the temporal coefficients.  $(\Phi_i)_{i \geq 1}$  are named modes.

## 2.2. POD mode properties

The spatial modes,  $(\Phi_i)$  are orthogonal and can be normalised:

$$(\Phi_i, \Phi_j) = \int_{\Omega} \Phi_i(x) \cdot \Phi_j(x) dx = \delta_{ij}. \quad (8)$$

This satisfies the boundary conditions. In case of an incompressible fluid, the velocity field fulfills the free divergence, i.e.  $\text{div } \Phi_i = 0$ .

The temporal coefficients  $a_i(t)$  are obtained from the projection of  $v$  onto the  $(\Phi_i)$  basis:

$$a_i(t) = (v(t), \Phi_i). \quad (9)$$

Moreover, they are not correlated and the eigenvalues are the temporal average

$$\langle a_i(t) a_j(t) \rangle = \delta_{ij} \lambda_i \quad (\text{without summation on the repeated indices}). \quad (10)$$

The eigenvalue  $\lambda_i$  is the energy captured by the mode  $\Phi_i$ . For a given  $N$ , the POD decomposition is the best energy decomposition that can be obtained.

## 2.3. The snapshot POD

Solving Eq. (2) can be computationally intensive in a higher dimensional problem. In order to minimise the computational time, the so-called snapshot method has been introduced by Sirovich (1987).

Let  $N_m$  be the number of nodes,  $n_c$  the number of components and  $\Phi$  a POD mode. If sampling of  $M$  realisations ( $MN_m n_c$ ) of the flow is enough to describe the problem, then we search the temporal coefficients  $a_k$ , such as

$$\Phi(x) = \sum_{k=1}^M A_k v(x, t_k). \quad (11)$$

Introducing the temporal average  $\langle \bullet \rangle$ , and using the inner product of  $\mathbf{L}^2(\Omega)$ , we have to solve the following eigenvalue problem:

$$\sum_{k=1}^M \frac{1}{M} (v(t_i), v(t_k)) A_k = \lambda A_i \quad \text{pour } i = 1, \dots, M. \quad (12)$$

Hence, the spatial modes  $\Phi_i$  are obtained from Eq. (11) and the temporal coefficients  $a_i$  are found by solving Eq. (9).

Earlier, the use of the classical or snapshot methods depended on the data type, but nowadays the problem size, due to the increased use of parallel computing, time is not a limiting factor. In the present study, the POD basis computed by the snapshot method has been used.

Note that, when a non-stationary problem is considered, another solution could be the bi-orthogonal decomposition (Aubry et al., 1991; Hémon and Santi, 2003).

#### 2.4. The bi-orthogonal decomposition (BOD)

The BOD was introduced by Aubry et al. (1991) in order to study spatio-temporal signals. The BOD consists in finding the decomposition of a signal with only one constraint that the signal could be square-integrable. In the same way as the POD, considering a signal  $v \in \mathbf{L}^2(\Omega \times \mathbf{T})$ ,  $x \in \Omega$ ,  $t \in \mathbf{T}$ ,  $\Omega \subset \mathbb{R}^3$  and  $\mathbf{T} \subset \mathbb{R}$ ;  $v$  can be written as the following bi-orthogonal decomposition:

$$v(x, t) = \sum_{k=1}^{\infty} \alpha_k \psi_k(t) \varphi_k(x). \tag{13}$$

A proof of this decomposition can be found in Aubry et al. (1991). It was also shown that

$$\alpha_1 \geq \alpha_2 \geq \dots \geq \alpha_0, \quad \lim_{M \rightarrow \infty} \alpha_M = 0,$$

$$(\varphi_k, \varphi_l)_{\mathbf{L}^2(\Omega)} = (\psi_k \psi_l)_{\mathbf{L}^2(\mathbf{T})} = \delta_{kl}. \tag{14}$$

The spatial modes  $\varphi_k(x)$  are named topos,  $\varphi_k \in \mathbf{L}^2(\Omega)$  and the temporal  $\psi_k(t)$ , chronos,  $\psi_k \in \mathbf{L}^2(\mathbf{T})$ . The topos and chronos associated to the eigenvalues  $\alpha_k^2 = \lambda_k$  are eigenvectors for the followings operators:

$$\mathbf{S}c(x, x') = \int_{\mathbf{T}} v(x, t) v(x', t) dt, \quad \mathbf{T}c(t, t') = \int_{\Omega} v(x, t) v(x, t') dx. \tag{15}$$

Hémon and Santi (2003) applied the BOD to study the wall-pressure distribution associated with an aerodynamic load. Couplet (2005) noted that using a discrete formulation of the BOD problem is a particular expression of the proper orthogonal decomposition (POD).

#### 2.5. POD application in fluid mechanics

In this section some general results obtained in the last decade in the field of reduced order modelling in fluid mechanics are presented.

Considering an incompressible fluid in a rigid domain  $\Omega$ , with the density  $\rho_f$  and the viscosity  $\mu_f$ , the fluid velocity  $v$  and the pressure  $p$  follow the dimensionless momentum equation of the flow:

$$\frac{\partial v}{\partial t} + v \cdot \nabla v = -\nabla p + \frac{1}{\text{Re}} \Delta v, \tag{16}$$

where Re is the Reynolds number.  $v$  is decomposed on the truncated POD basis at  $N$  modes:

$$v \approx v^N = \sum_{k=1}^N a_k(t) \Phi_k(x). \tag{17}$$

The velocity decomposition (17) is introduced in Eq. (16) and projected onto the POD vector  $\Phi_n$ . Thanks to the orthogonality and the free divergence of the POD basis  $\Phi$ , the following system has been obtained:

$$\frac{da_n}{dt} = \sum_{k=1}^N \sum_{l=1}^N a_k a_l C_{kln} + \sum_{k=1}^N a_k B_{kn} + D_n \quad \text{with } n = 1 \dots N, \tag{18}$$

where

$$C_{kln} = -(\Phi_k \cdot \nabla \Phi_l, \Phi_n) = \int_{\Omega} (\Phi_k \cdot \nabla \Phi_l) \cdot \Phi_n dx, \tag{19}$$

$$B_{kn} = \frac{1}{\text{Re}} (\Phi_k, \Phi_n) = \int_{\Omega} \Phi_k \cdot \Phi_n dx, \tag{20}$$

$$D_n = - \int_{\partial\Omega} p \Phi_n \cdot \mathbf{n}_f dx, \tag{21}$$

with  $\mathbf{n}_f$  being the outward normal of the domain  $\Omega$  considered for the boundary  $\partial\Omega$ .

The coefficient  $D_n$  which contains the pressure term  $p$  can be avoided. Indeed, for more cases (for example the driven cavity) the velocity field is equal to zero on the boundary, and, as the POD vector complies with homogeneous boundary conditions,  $D_n$  is zero. In other cases, some particular methods have been developed. Refer to Rempfer (1996), who uses a vorticity formulation. Aubry et al. (1988) modelled this term for the study of the viscous sublayer in a channel flow and Allery (2002) uses a penalisation method. This method will be explained in the following paragraph.

The term  $\int_{\Gamma_f} p \Phi_n \cdot \mathbf{n}_f dx$  is avoided by a stress formulation in conjunction with a penalisation of the non-homogeneous Dirichlet boundary conditions (Allery, 2002). This method considers the following strain boundary condition on the non-zero velocity fluid boundary  $\Gamma_f$ :

$$\boldsymbol{\sigma} \cdot \mathbf{n} = F = G(v|_{\Gamma_\sigma} - v^{BC}),$$

where  $v|_{\Gamma_\sigma}$  denotes the velocity computed on  $\Gamma_\sigma$ ,  $v^{BC}$  the velocity imposed and  $G$  a constant. Choosing  $G$  relatively larger than  $\|F\|$  leads to consider that

$$v|_{\Gamma_\sigma} - v^{BC} = \frac{F}{G} \rightarrow 0.$$

Thus, an  $N$  th order dynamical system is obtained (Eq. (18)). It consists in solving an ordinary differential equation system in time with the coefficients  $B$ ,  $C$ ,  $D$ , which are independent of time and are computed only once. In the practice,  $N$  is of order 10, that is why this system is referred to as a low-order dynamical system. Aubry et al. (1988) constructed the first model to study the motion of turbulent structures on a flat plate. Later, various configurations have been studied, for example near a wall boundary layer (Rempfer, 1996; Rempfer and Fasel, 1994), channel flow (Deane et al., 1991; Omurtag and Sirovich, 1999) and driven cavity flow (Cazemier et al., 1998). Further examples are in Berkooz et al. (1993) and Holmes et al. (1997).

One example on the effectiveness of this method is given by Allery et al. (2004, 2005), who applied a method to study the Coanda effect (Allery et al., 2004) and to model the fluid flow for computation of particle dispersion in a two-dimensional ventilated cavity (Allery et al., 2005). Allery et al. (2004) propose that for the Coanda effect six modes are sufficient to completely capture the spatial structure of the flow and to obtain a good reconstruction with a low-order dynamical system. In the second article, Allery et al. (2005) indicate that only four modes are necessary to obtain a residual between the reconstructed velocity and the snapshot velocity less than  $1.8 \times 10^{-2}$ .

### 3. POD application in fluid–structure interaction

#### 3.1. Mathematical formulation

In the foregoing the application of the POD method in the field of fluid mechanics has been presented. A low-order dynamical system has been obtained by projecting the Navier–Stokes equations on the POD basis, which is a spatial basis, truncated at  $N$  modes. This method cannot be applied in fluid–structure interaction for the fluid velocity field; the fluid domain being time variant and the POD basis being spatial, thus are not time-dependent. The problem considered can be illustrated by the computation of the POD vectors by the snapshot method. Considering a time-variant domain  $\Omega_f$  and  $M$  snapshot of a velocity field  $v$ , which is defined on  $\Omega_f$ . The snapshot problem needs building the snapshot matrix, i.e the matrix  $\mathbf{C}$  composed of  $c_{ij}$ , where

$$c_{ij} = (v(\bullet, t_i), v(\bullet, t_j)) = \int_{\Omega_f} v(x, t_i) \cdot v(x, t_j) dx, \quad i, j = 1, \dots, M.$$

How to define the  $\Omega_f$  domain if the fluid domain is different at different time steps ( $t_i$  and  $t_j$ )?

A few articles deal with the POD application for a general case of moving boundary problems and less for fluid–structure interaction problems. In case of moving boundary problems, the POD is applied for a vector velocity field by Anttonen et al. (2005, 2003) using a discrete scalar product, i.e.  $(u(\bullet, t), v(\bullet, t)) = \sum_{i=1}^{N_n} u(x_i, t)v(x_i, t)$ , where  $x_i$  denotes a node of the moving grid and  $N_n$  the number of nodes. Consequently, the information about the moving domain is lost. Lieu et al. (2006) applied successfully POD-ROM for a complete aircraft configuration. In this last case, the low-order dynamical system has been built by projecting the linearised finite element formulation on the POD basis.

A standard snapshot POD method, computing the POD modes by the discrete scalar product, has been tested by Liberge (2008), and by Liberge et al. (2007) on a one-dimensional case of the Burgers equation coupled with a spring. The low-order dynamical system was obtained by projecting the initial discrete problem to the POD basis. The solution

proposed by Liberge et al. (2007) gave better results. We propose in this article an extension of the method presented by Liberge et al. (2007) for the interaction between turbulent fluid flow and structures.

### 3.2. Proposed solution

This article proposes a new method to obtain a low-order dynamical system with a nonlinear formulation. The first step consists in building a POD basis. Utturkar et al. (2005) used a fixed uniform grid to compute POD modes around a membrane wing. The fluid velocity field is interpolated from the time-variant grid to a fixed uniform one, and the POD basis is computed on the fixed grid. We propose to extend the method for the case of a moving solid body by considering a fixed uniform grid containing all the time-variant grid (fluid and solid), and then interpolating the fluid and the solid velocity field from the time variant grid to the fixed uniform one. Next, the POD basis is computed for the global velocity field  $v$  (fluid and solid) on the fixed uniform grid. Then, a characteristic function is introduced to follow the different domains. This method has been used by Liberge et al. (2007) for the POD application for fluid–structure interaction problems.

Fig. 1 shows a schematic description of the problem domain of interest, where  $\Omega_s(t)$  is the domain occupied by the moving body;  $\Omega_f(t)$  is the moving spatial domain upon which the fluid motion is described;  $\Gamma_I(t)$  is the interface between  $\Omega_s(t)$  and  $\Omega_f(t)$ , and  $\mathbf{n}$  the outward normal of  $\Omega_s$ .

For practical reasons, a rigid body has been considered. As the rigid body  $\Omega_s(t)$  changes position, the interface  $\Gamma_I(t)$  moves accordingly. We note  $\Omega = \Omega_f(t) \cup \Omega_s(t) \cup \Gamma_I(t)$ .

The global velocity field denoted by  $v$ , is decomposed as

$$\forall x \in \Omega, \quad v(x, t) = v_f(x, t)\mathbb{1}_{\Omega_f}(x, t) + v_s(x, t)(1 - \mathbb{1}_{\Omega_f}(x, t)), \tag{22}$$

where  $v_f$  denotes the fluid velocity field,  $v_s$  the solid, and  $\mathbb{1}_{\Omega_f}$  the characteristic function of the fluid domain:

$$\mathbb{1}_{\Omega_f}(x, t) = \begin{cases} 1 & \text{if } x \in \Omega_f(t), \\ 0 & \text{if else.} \end{cases} \tag{23}$$

A non-sliding condition has been considered at the fluid–solid interface  $\Gamma_I$ , i.e.

$$v_f = v_s \quad \text{on } \Gamma_I,$$

$$\sigma_f \cdot \mathbf{n} = \sigma_s \cdot \mathbf{n} \quad \text{on } \Gamma_I. \tag{24}$$

This method is equivalent to considering the solid domain as Eulerian. Different methods have been presented in the literature. The most famous is the Immersed Boundary Method introduced by Peskin (1973) which leads to a few derivative methods. This method consists in modelling the solid by a membrane immersed in a fluid flow. This membrane is take into account by adding a force term to the fluid equation and next, the fluid constraint is interpolated on the membrane. One of the main issues is the non-physical representation of the fluid–solid interface. That is why the

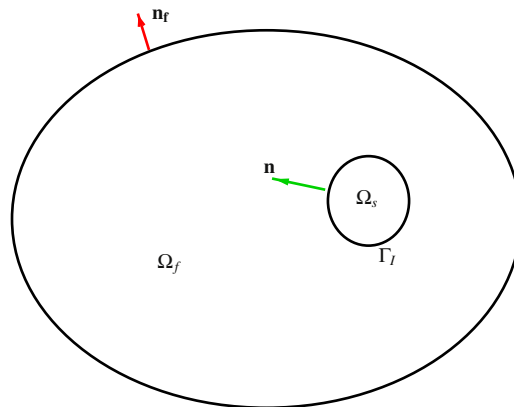


Fig. 1. Schematic description of the problem domain.

authors propose an alternate method, the so-called fictitious domain method developed for fluid–solid–rigid interaction problems by Glowinski et al. (1999) and Patankar et al. (2000).

The fictitious domain method developed by Patankar et al. (2000) consists in treating the entire fluid–solid rigid domain (the fictitious domain) as a fluid, by extending the Navier–Stokes equations to the solid rigid domain and adding the following rigid constraint:

$$\mathbf{D}(v) = \frac{1}{2}(\nabla v + \nabla^T v) = 0 \quad \text{in } \Omega_s. \quad (25)$$

This constraint is penalised in the variational formulation by a viscosity  $\mu_s$  with a Lagrange multiplier  $\lambda$  associated with it. It leads to the following variational formulation:

$$\mathbf{H}_{v_f} = \{v | v \in \mathbf{H}^1(\Omega), v = v_f(t) \text{ on } \partial\Omega \setminus \Gamma_I\},$$

$$\mathbf{H}_0 = \{v | v \in \mathbf{H}(\Omega), v = 0 \text{ on } \partial\Omega \setminus \Gamma_I\},$$

$$\mathbf{L}_0^2(\Omega) = \left\{ q \in \mathbf{L}^2(\Omega) \left| \int_{\Omega} q \, dx = 0 \right. \right\}, \quad (26)$$

$\forall v^* \in \mathbf{H}_0$  and  $q \in \mathbf{L}^2(\Omega)$ , find  $v \in \mathbf{H}_{v_f}$ ,  $p \in \mathbf{L}_0^2(\Omega)$ ,  $\lambda \in \mathbf{H}^1(\Omega_s(t))$ , such that

$$\int_{\Omega} \rho \left( \frac{\partial v}{\partial t} + v \cdot \nabla v \right) \cdot v^* \, dx - \int_{\Omega} p \nabla \cdot v^* \, dx + \int_{\Omega} q \nabla \cdot v \, dx + \int_{\Omega} 2\mu \mathbf{D}(v) : \mathbf{D}(v^*) \, dx + \int_{\Omega_s(t)} \mathbf{D}(\lambda) : \mathbf{D}(v^*) \, dx = 0. \quad (27)$$

$\rho$  and  $\mu$  are defined on the global domain  $\Omega$ :

$$\rho = \mathbb{1}_{\Omega_f} \rho_f + (1 - \mathbb{1}_{\Omega_f}) \rho_s, \quad \mu = \mathbb{1}_{\Omega_f} \mu_f + (1 - \mathbb{1}_{\Omega_f}) \mu_s, \quad (28)$$

where  $\rho_f$  is the fluid density,  $\mu_f$  the fluid viscosity and the solid viscosity  $\mu_s$  is the penalisation factor of the rigidity constraint and  $\Gamma_f = \partial\Omega_f \setminus \Gamma_I$ ;  $\rho_s$  is the solid density,  $\mathbf{D}(v) = 0$  denotes the rigid constraint, and  $v_f$  the velocity fluid at the fluid–structure interface.

Thus a weak formulation is obtained for the global domain  $\Omega$  with information about the fluid and solid domain that is contained in the density  $\rho$  and viscosity  $\mu$  functions.

The other advantage of this formulation is that the computation of the forces on the solid interface is quite unnecessary. Indeed, considering the integration of the  $\sigma_s$  tensor on the solid domain, and  $v_s^*$  a virtual field, the following expression is obtained:

$$\int_{\Omega_s} (\nabla \cdot \sigma_s) \cdot v_s^* \, dx = \int_{\Gamma_I} (\sigma_s \cdot \mathbf{n}) \cdot v_s^* \, dx - \int_{\Omega_s} \mathbf{Tr}(\sigma_s \mathbf{D}(v_s^*)) \, dx. \quad (29)$$

For a rigid velocity field, on  $\Omega_s$ ,  $\mathbf{D}(v_s^*) = 0$ , and taking into account conditions (24), Eq. (29) can be written as

$$\int_{\Omega_s} (\nabla \cdot \sigma_s) \cdot v_s^* \, dx = \int_{\Gamma_I} (\sigma_f \cdot \mathbf{n}) \cdot v_s^* \, dx. \quad (30)$$

The same operations have been made for  $\sigma_f$  on the domain  $\Omega_f$ ,

$$\int_{\Omega_f} (\nabla \cdot \sigma_f) \cdot v_f^* \, dx = - \int_{\Gamma_I} \sigma_f \mathbf{n} \cdot v_f^* \, dx - \int_{\Omega_f} \mathbf{Tr}(\sigma_f \mathbf{D}(v_f^*)) \, dx + \int_{\Gamma} \sigma_f \mathbf{n}_f \cdot v_f^* \, dx, \quad (31)$$

where  $\mathbf{n}$  is the outward normal of the solid domain.

By adding Eqs. (31) and (32) the term on the interface  $\Gamma_I$  gets cancelled:

$$\int_{\Omega} (\nabla \cdot \sigma) \cdot v^* \, dx = - \int_{\Omega} \mathbf{Tr}(\sigma \mathbf{D}(v^*)) \, dx + \int_{\Gamma} \sigma_f \mathbf{n}_f \cdot v^* \, dx, \quad (32)$$

where  $\sigma = \mathbb{1}_{\Omega_f} \sigma_f + (1 - \mathbb{1}_{\Omega_f}) \sigma_s$  and  $v^* = \mathbb{1}_{\Omega_f} v_f^* + (1 - \mathbb{1}_{\Omega_f}) v_s^*$ .

### 3.3. Low-order dynamical system

#### 3.3.1. First approach

The low-order dynamical system has been obtained by choosing POD modes  $\Phi_i, i = 1, \dots, N$  for a virtual velocity field.

$N$  is sought as  $\sum_{i=1}^N \lambda_i / \sum_{i=1}^M \lambda_i > \alpha$ ,  $\alpha > 0.9999$ , where  $\lambda_i$  denotes the  $i$  th eigenvalue of the POD problem, and  $M$  the snapshot number. Thus, the velocity field  $v$  is evaluated by using this truncated basis as Eq. (17)

$$v = \sum_{i=1}^N a_i(t) \Phi_i(x).$$

This decomposition is introduced in (27) and the following dynamical system is obtained:  $\forall t \in [0, T]$  for  $n = 1, \dots, N$ ,

$$\begin{cases} \sum_{i=1}^N \frac{da_i}{dt} A_{in}^t + \sum_{i=1}^N \sum_{j=1}^N a_i(t) a_j(t) B'_{ijn} + \sum_{i=1}^N a_i(t) C_{in}^t + E_n^t = 0, \\ \frac{\partial \mathbb{ll}_{\Omega_f}}{\partial t} + v \cdot \nabla \mathbb{ll}_{\Omega_f} = 0, \end{cases} \quad (33)$$

with

$$A_{in}^t = \int_{\Omega} \rho(x, t) \Phi_i(x) \cdot \Phi_n(x) \, dx, \quad B'_{ijn} = \int_{\Omega} \rho(x, t) (\nabla \Phi_i \cdot \Phi_j) \cdot \Phi_n \, dx,$$

$$C_{in}^t = 2 \int_{\Omega} \mu(x, t) \mathbf{tr}(\mathbf{D}(\Phi_i) \cdot \mathbf{D}(\Phi_n)) \, dx - \int_{\Gamma_f} 2\mu_f(\mathbf{D}(\Phi_i)\Phi_n) \cdot \mathbf{n} \, dx,$$

$$E_n^t = \int_{\Omega_s} \mathbb{ll}_{\Omega_s}(x, t) \mathbf{tr}(\mathbf{D}(\lambda)\mathbf{D}(\Phi_n)) \, dx - \int_{\Gamma_l} (\mathbf{D}(\lambda)\Phi_n) \cdot \mathbf{n} \, dx + \int_{\Gamma_f} p\Phi_n \cdot \mathbf{n} \, dx.$$

There are some differences compared to the low-order dynamical system obtained using POD basis in classical fluid mechanics as presented in Section 2.5. In fact, coefficients  $A$ ,  $B$ , etc. are time-variant and must be computed at each time step. The computational cost at each time step should be considered as a limitation of the method, but in fact for a small number of POD modes the computational expense is smaller as compared to that of a FSI problem solved with the ALE method. This method does not require a remeshing step; also, the initial problem is transformed into a low-order set of ordinary differential equation.

### 3.3.2. Second approach

The computational time can also be reduced by construction of a system with time-independent coefficients. The decomposition of the characteristic function  $\mathbb{ll}_{\Omega_f}$  on a POD basis  $\Phi_i^c$ , and the decomposition of the Lagrange multiplier on the same basis of the velocity field yields the following:

$$\mathbb{ll}_{\Omega_f}(x, t) = \sum_{i=1}^{N_{fc}} b_i(t) \Phi_i^c(x), \quad (34)$$

$$\lambda(x, t) = \sum_{i=1}^{N_l} c_i(t) \Phi_i(x). \quad (35)$$

$N_{fc}$  and  $N_l$  denote the number of POD modes retained for the characteristic function and the Lagrange multiplier. In fact,  $N_l$  is chose equal to  $N$ .

This leads to the following dynamical system:  $\forall i = 1, \dots, N$ ,  $p = 1, \dots, N_c$ ,

$$\begin{aligned} \rho_f \frac{da_n}{dt} + (\rho_s - \rho_f) \sum_{k=1}^N \sum_{p=1}^{N_c} \frac{da_k}{dt} b_p \mathcal{A}_{pkl} + \rho_f \sum_{k=1}^N \sum_{l=1}^N a_k a_l \mathcal{B}_{kln}^1 + (\rho_s - \rho_f) \sum_{k=1}^N \sum_{l=1}^N \sum_{p=1}^{N_c} a_k a_l b_p \mathcal{B}_{pkn}^2 \\ + 2\mu_f \sum_{k=1}^N a_k \mathcal{C}_{kn}^1 + 2(\mu_s - \mu_f) \sum_{k=1}^N \sum_{p=1}^{N_c} a_k b_p \mathcal{C}_{kpn}^2 = \sum_{h=1}^{N_l} \sum_{p=1}^{N_c} b_p c_h \mathcal{D}_{phn}. \end{aligned} \quad (36)$$

$$\frac{db_p}{dt} + \sum_{k=1}^N \sum_{l=1}^{N_c} a_k b_l \mathcal{E}_{klp} = 0, \quad \sum_{p=1}^{N_c} \sum_{k=1}^N b_p a_k \mathcal{F}_{pkn} = 0, \quad (37a, b)$$

$$\begin{aligned}
\mathcal{A}_{pkl} &= \int_{\Omega} \Phi_p^{fc} \Phi_k \Phi_l \, dx, & \mathcal{C}_{kpm}^2 &= \int_{\Omega} \Phi_p^{fc} \mathbf{Tr}(\mathbf{D}(\Phi_k) \mathbf{D}(\Phi_m)) \, dx, \\
\mathcal{B}_{klm}^1 &= \int_{\Omega} (\Phi_k \nabla \Phi_l) \cdot \varphi_m \, dx, & \mathcal{C}_{kn}^1 &= \int_{\Omega} \mathbf{Tr}(\mathbf{D}(\Phi_k) \mathbf{D}(\Phi_n)) \, dx, \\
\mathcal{B}_{klpm}^2 &= \int_{\Omega} \Phi_p^{fc} (\Phi_k \nabla \Phi_l) \cdot \varphi_m \, dx, & \mathcal{D}_{phm} &= \int_{\Omega} \Phi_p^{fc} \mathbf{Tr}(\mathbf{D}(\Phi_h) \mathbf{D}(\Phi_m)) \, dx, \\
\mathcal{E}_{klp} &= \int_{\Omega} (\Phi_k \cdot \nabla \Phi_l^{fc}) \Phi_p^{fc} \, dx, & \mathcal{F}_{pkn} &= \int_{\Omega} \Phi_p^{fc} \mathbf{Tr}(\mathbf{D}(\Phi_k) \mathbf{D}(\Phi_n)) \, dx.
\end{aligned} \tag{38}$$

Eq. (37a) is the reduction of the diffusion equation of the characteristic function and Eq. (37b) is the reduction of Eq. (25). Thus, an algebraic differential equation system, whose coefficients can be computed once, is obtained.

In the present study, two low-order dynamical systems, which transformed the initial problem into a simpler system of ordinary differential equation in  $a_i(t)$  with fewer degrees of freedom have been presented. In practice the POD method gives a basis which is maximal in terms of energy, with only a few functions. The methods will be compared in the next section.

## 4. Application

### 4.1. Presentation

These methods have been tested on the configuration described in Fig. 2, a cylindrical rigid solid, attached to a spring, has been immersed in a fluid flow at Reynolds number  $Re = 1690$ .

For the fluid parameters, we consider the fluid density  $\rho_f = 1000 \, \text{kg m}^{-3}$ , the viscosity  $\mu_f = 0.001 \, \text{kg/m s}$ , the inlet velocity  $V_0 = 3.38 \times 10^{-2} \, \text{m s}^{-1}$ . The solid parameters are the radius  $R = 0.025 \, \text{m}$ , the mass equal to  $m_s = 11.78 \times 10^{-1} \, \text{kg}$ , which implies a solid density equal to  $\rho_s = 60 \, \text{kg m}^{-3}$ . The stiffness of the spring was chosen equal to  $k = 0.559 \, \text{N m}^{-1}$  and the damping to  $2.7825 \, \text{kg s}^{-1}$ .

The cylinder was considered blocked along the  $x_1$  axis, and oscillated due to the fluid forces along the other axis. The snapshot solution has been computed by the software STARCD with a variant RANS turbulence model ( $\kappa-\omega$ ) using the ALE method (Longatte et al., 2009, 2003) to adapt the mesh around the moving rigid body. The solid movement equations are computed by a sub-programme, integrated into the CFD code. The two domains (fluid and solid) are coupled by a semi-implicit coupled algorithm (Abouri et al., 2006). One hundred and fifty snapshots of the solution are taken during one cylinder oscillation period and are interpolated on a regular grid (the discretisation step is  $6.52 \times 10^{-3} \, \text{m}$  according to the first axis and  $5.025 \times 10^{-3} \, \text{m}$  according to the second), in a way that 10 nodes are along the diameter of the cylinder. The two first POD modes are illustrated in Fig. 3.

The first POD mode looks like the temporal average velocity field, and the other modes capture the velocity fluctuations around this average. In practice, when this situation is observed, the velocity field is decomposed as a temporal average term  $\langle v \rangle$  and a fluctuation  $v'(x, t)$ . The POD vectors  $\Phi'$  are sought for  $v'$  instead of  $v$ . The low-order

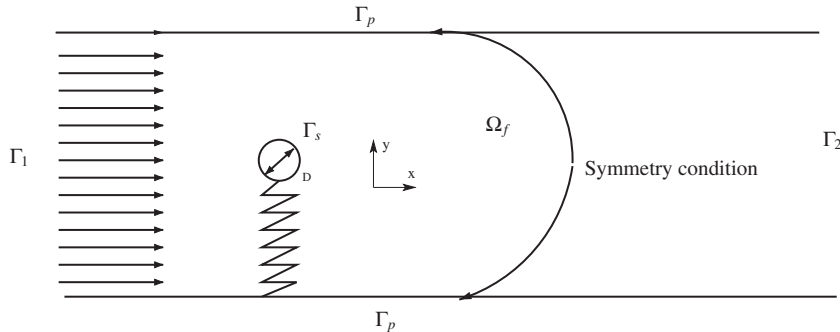


Fig. 2. Schematic description.

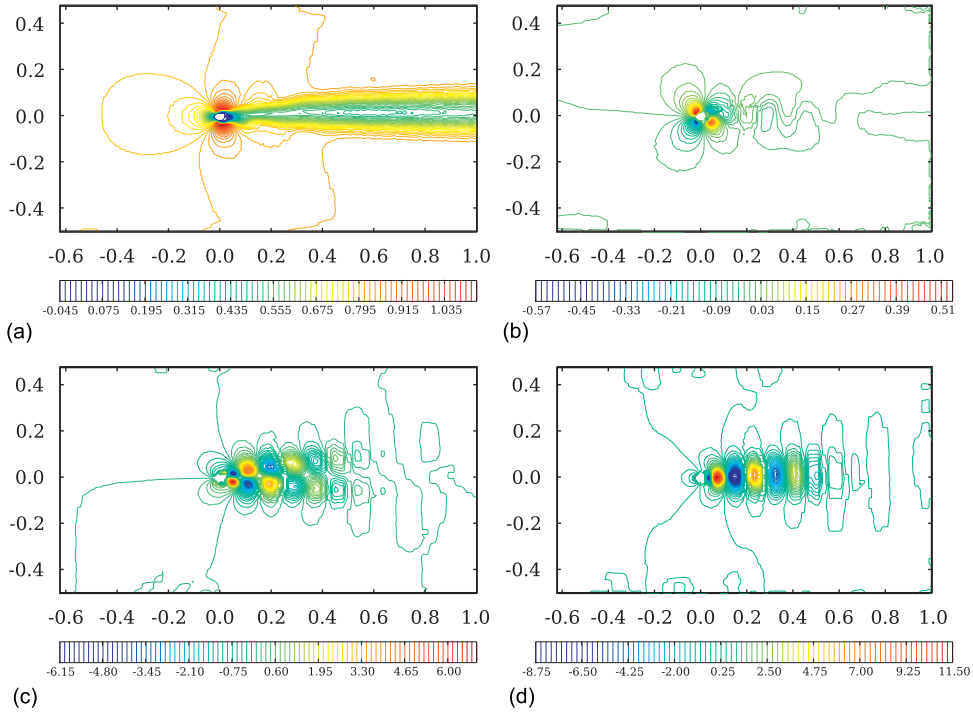


Fig. 3. Isovalues of the two first POD modes. (a) First component of  $\Phi_1$ ; (b) second component of  $\Phi_1$ ; (c) first component of  $\Phi_2$ ; (d) second component of  $\Phi_2$ .

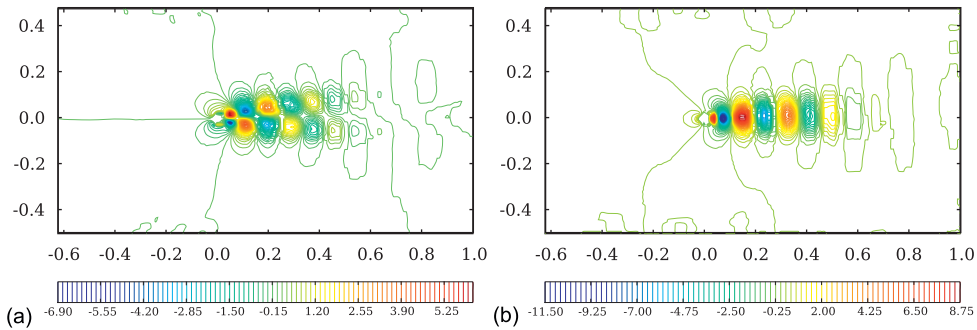


Fig. 4. Isovalues of the first POD mode obtained for  $v'$ . (a) First component of  $\Phi'_1$ ; (b) second component of  $\Phi'_1$ .

dynamical system obtained is similar to (33); the velocity field decomposed as

$$v(x, t) = \langle v(x) \rangle + v'(x, t) = \langle v(x) \rangle + \sum_{i=1}^N a'_i(t) \Phi'_i(x), \quad (39)$$

and the projection basis  $\Phi'_i$ ,  $i = 1, \dots, N$  instead of  $\Phi_i$ ,  $i = 1, \dots, N$ .

The same results have been obtained as in the field of fluid mechanics using POD method, i.e. the first POD mode obtained for  $v'$  corresponds to the second obtained for  $v$  (Fig. 4).

The energy convergence is plotted on Fig. 5. The function

$$f(k) = \left( \sum_{i=1}^k \lambda_i \right) / \left( \sum_{j=1}^M \lambda_j \right), \quad (40)$$

where  $k$  is the number of POD modes used and  $M$  the total number of modes computed, is the energy captured with the  $k$  first modes. The quasi-totality of energy is captured with only 6 POD modes.

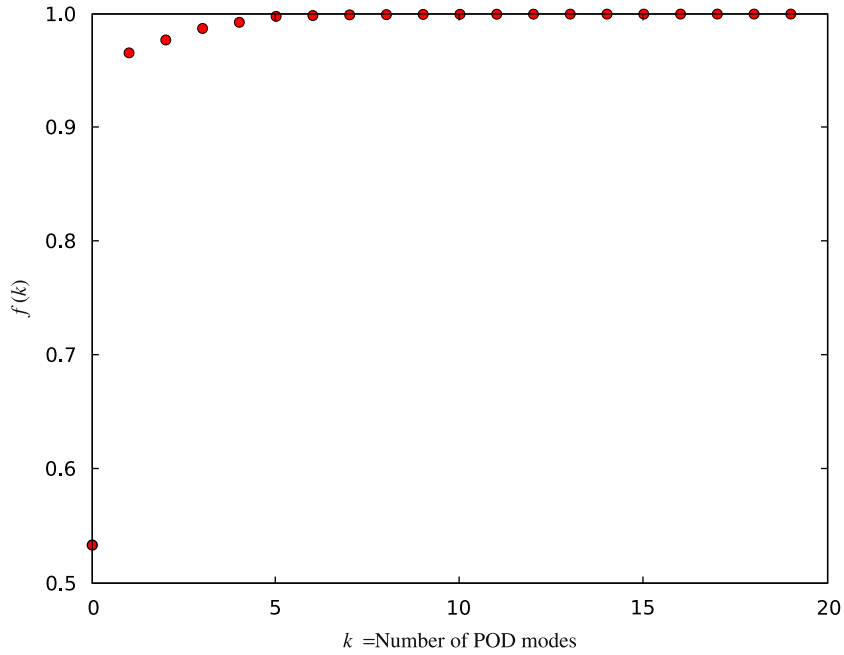


Fig. 5. Energy convergence per mode.

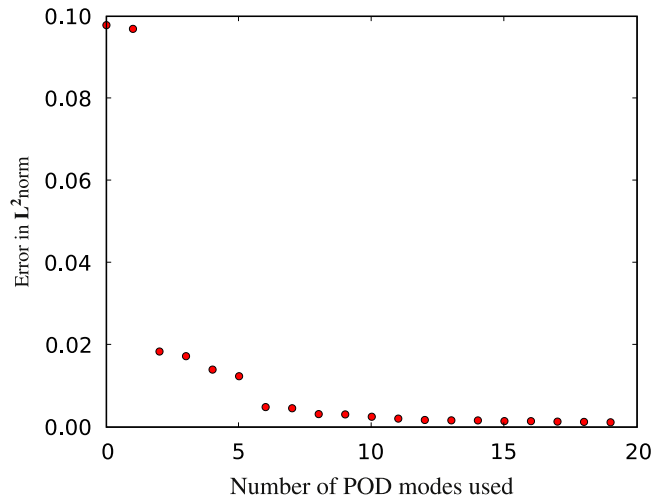


Fig. 6. Reconstruction error versus number of POD modes used.

#### 4.2. POD analysis

First, the POD reconstruction of the velocity field has been evaluated by the direct POD method. It consists in computing the temporal coefficients by projecting each snapshot onto the POD basis:

$$\text{for } k = 1, \dots, M \quad a_{i=1}^d(t_k) = (v'(\bullet, t_k), \Phi_i'), \quad i = 1, \dots, N. \quad (41)$$

Fig. 6 shows the development of the velocity reconstruction error in  $L^2$  norm according the number  $N$  of modes used in Eq. (39). Three POD modes are sufficient to reconstruct the velocity field with an error less than 2%. However, with 2

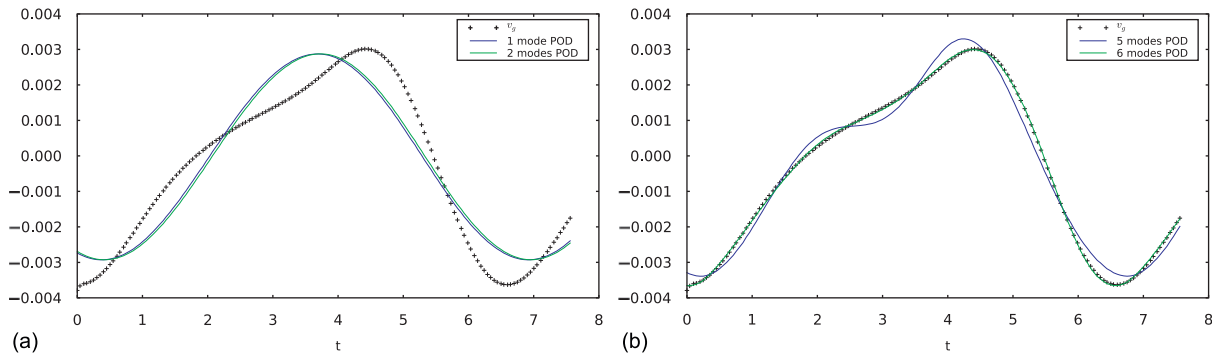


Fig. 7. Second component of the velocity on the gravity centre of the rigid body: initial and reconstructed. (a) With 1 and 2 modes; (b) with 5 and 6 modes.

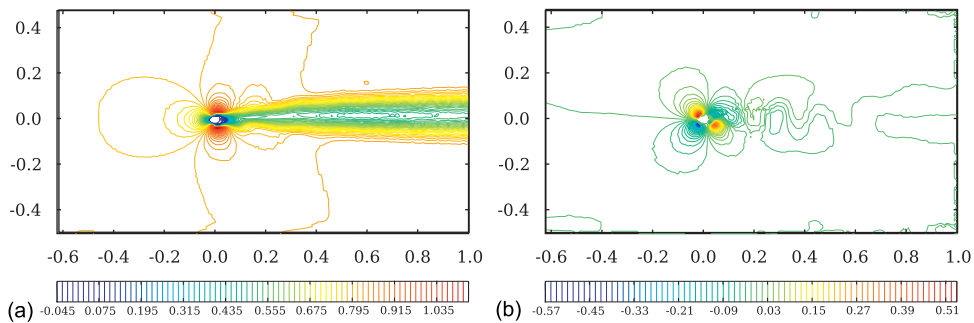


Fig. 8. Isovalues of the first topos obtained for  $v$ . (a) First component of  $\Phi_1$ ; (b) second component of  $\Phi_1$ .

Table 1  
Comparison of CPU times.

	STARCD ALE	LODS (33)	LODS (36)
CPU time	726	143	21

POD modes the reconstruction of the velocity on the gravity centre of the rigid body is not satisfactory (Fig. 7(a)). The objective of this work is to reconstruct the velocity field and the solid displacement, that is why more modes have been added. Fig. 7(b) shows that 6 POD modes are enough to reconstruct the velocity field at the solid gravity centre.

This number is sufficient regarding the literature of POD study of a cylinder. In case of turbulent flow around a fixed cylinder at a Reynolds number of 140 000 (Perrin et al., 2006) considered that 10 POD modes are sufficient to obtain the essential of the von Karman vortices.

The BOD (Aubry et al., 1991; Hémon and Santi, 2003) has already been tested and it has been shown by Liberge (2008) that the results obtained are the same (Fig. 8).

### 4.3. Reduced Order Modelling

The low-order dynamical systems are built with 6 POD modes. Table 1 compares the computational time using the STARCD software, for the first low-order dynamical system (LODS) (33) and the second LODS (36).

The last proposed solution is the faster. The first gives a gain in terms of computational time, but the computational cost of the coefficients at each time step is more important. The gain in terms of CPU times obtained with the system LODS (36) is significant.

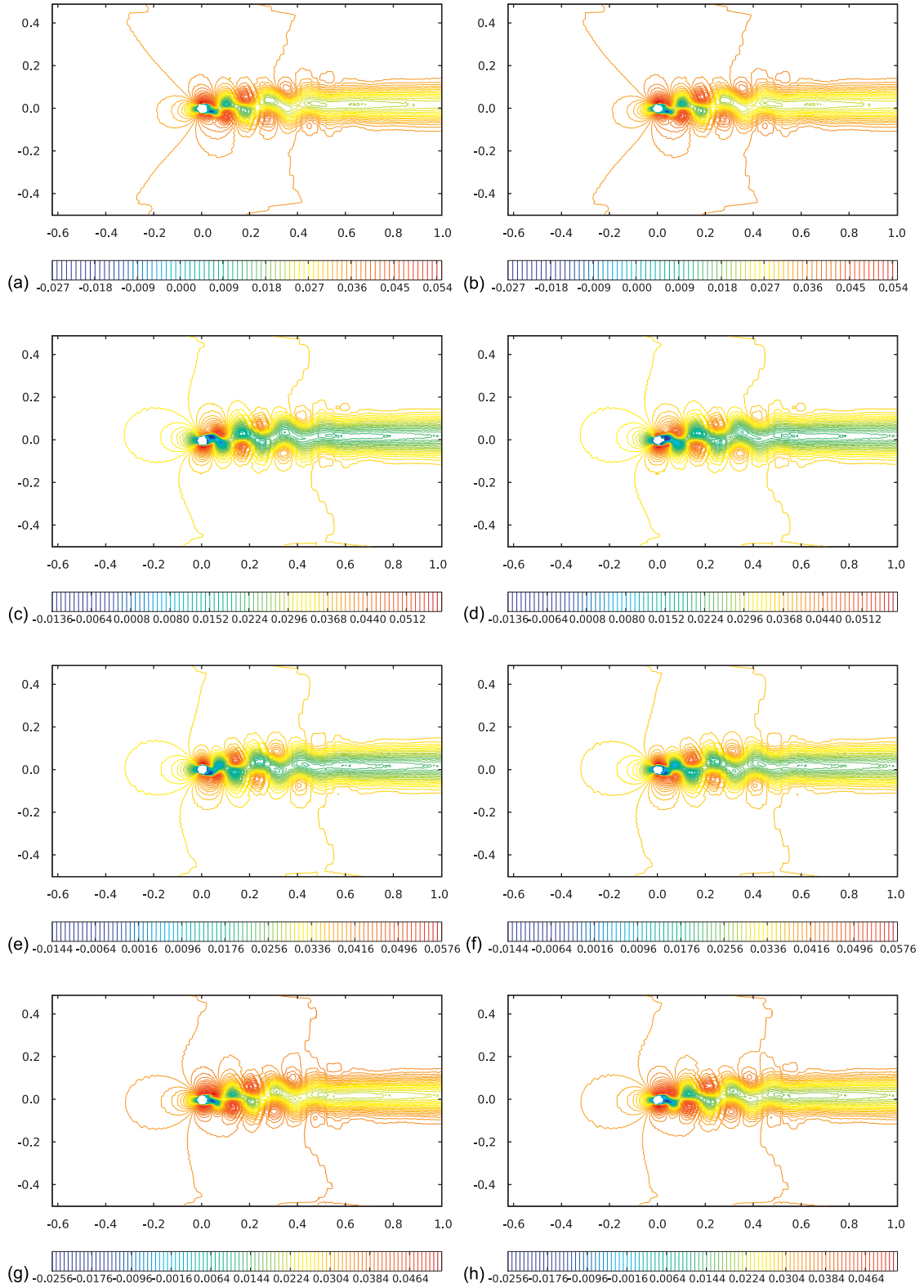


Fig. 9. First component of the velocity field. Left: snapshot velocity field; right: obtained by low-order dynamical system. (a)  $v(1, 1)$ ; (b)  $\psi(1, 1)$ ; (c)  $v(50, 1)$ ; (d)  $\psi(50, 1)$ ; (e)  $v(100, 1)$ ; (f)  $\psi(100, 1)$ ; (g)  $v(150, 1)$ ; (h)  $\psi(150, 1)$ .

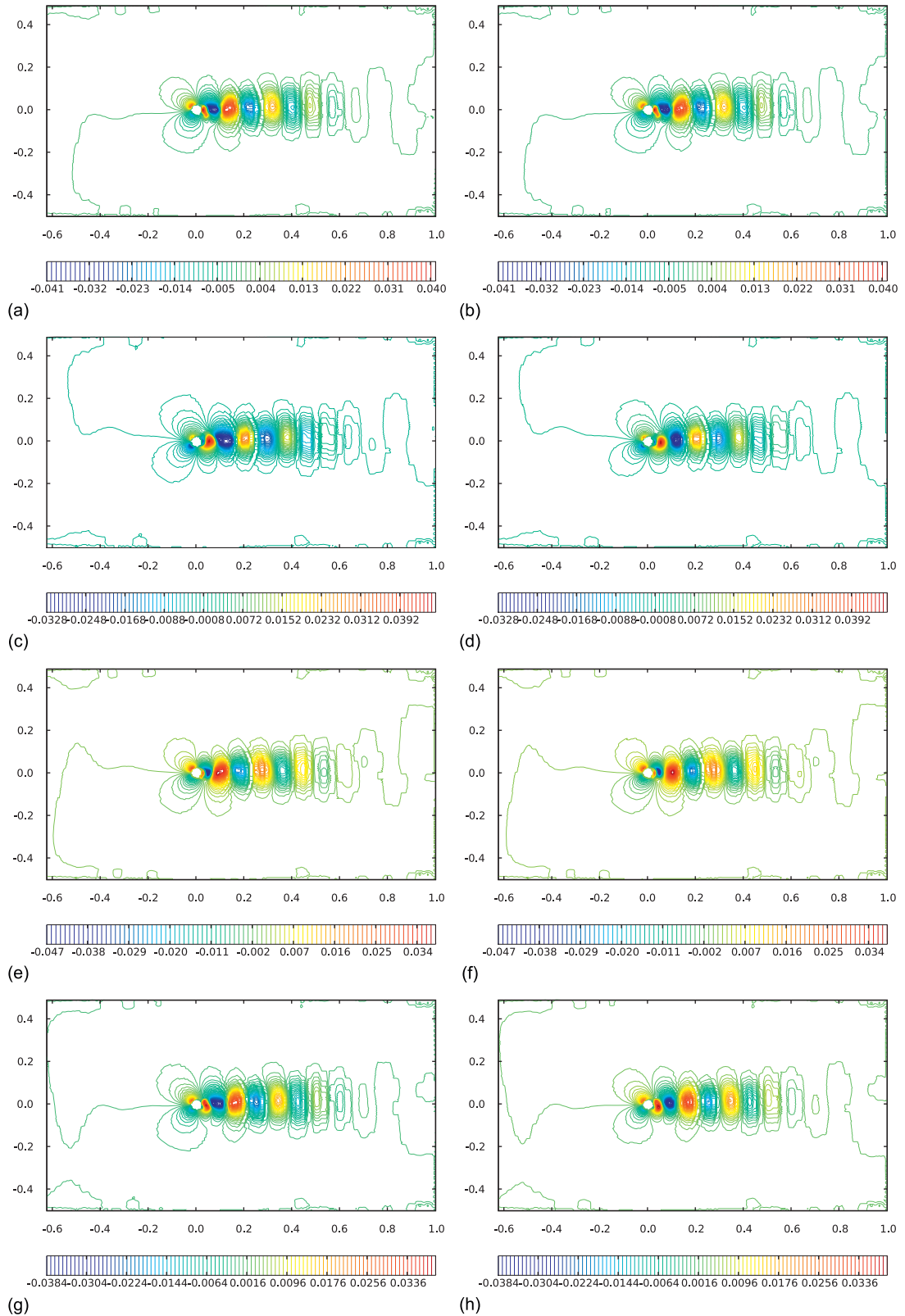


Fig. 10. Second component of the velocity field. Left: snapshot velocity field; right: obtained by low-order dynamical system. (a)  $v(1, 2)$ ; (b)  $\psi(1, 2)$ ; (c)  $v(50, 2)$ ; (d)  $\psi(50, 2)$ ; (e)  $v(100, 2)$ ; (f)  $\psi(100, 2)$ ; (g)  $v(150, 2)$ ; (h)  $\psi(150, 2)$ .

Figs. 9 and 10 compare the snapshots and solutions reconstructed using the temporal coefficients obtained by the low-order dynamical system (36) at four different time steps;  $v(T, i)$  denotes the  $i$  component of the  $T$  snapshot of the velocity field and  $\psi(T, i)$  the corresponding velocity field reconstructed using the solution of the low-order dynamical system.

A good fit is found for the velocity field. The obtained velocity field compares well with the existing results.

Another comparison has been made on the vorticity (Fig. 11) and the viscous stress (Figs. 12–14) and on the Reynolds stress (Figs. 15–17).

For the vorticity, the same shedding is observed.

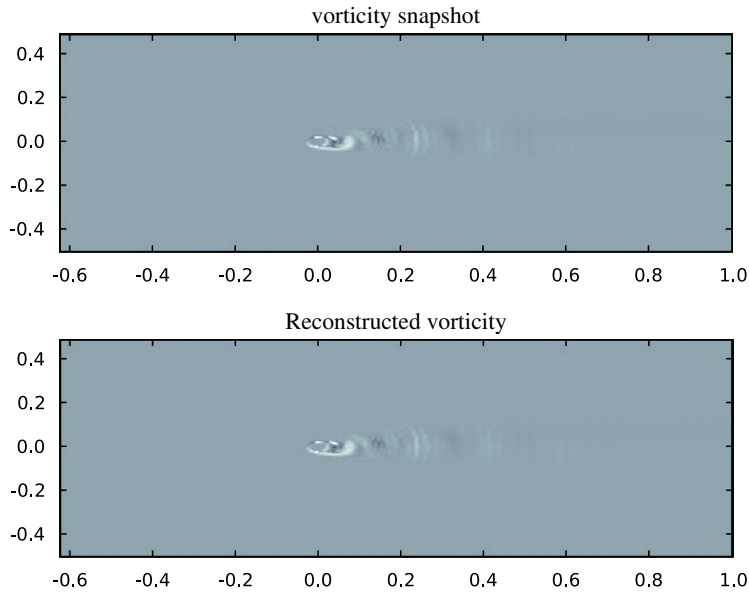


Fig. 11. Comparison of the 110th snapshot vorticity and those reconstructed.

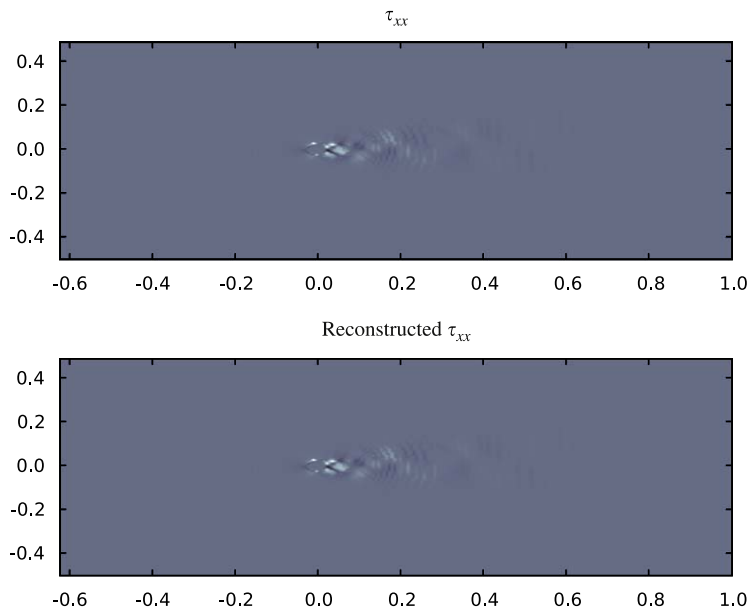


Fig. 12. Comparison of the 110th snapshot  $\tau_{xx}$  and those reconstructed.

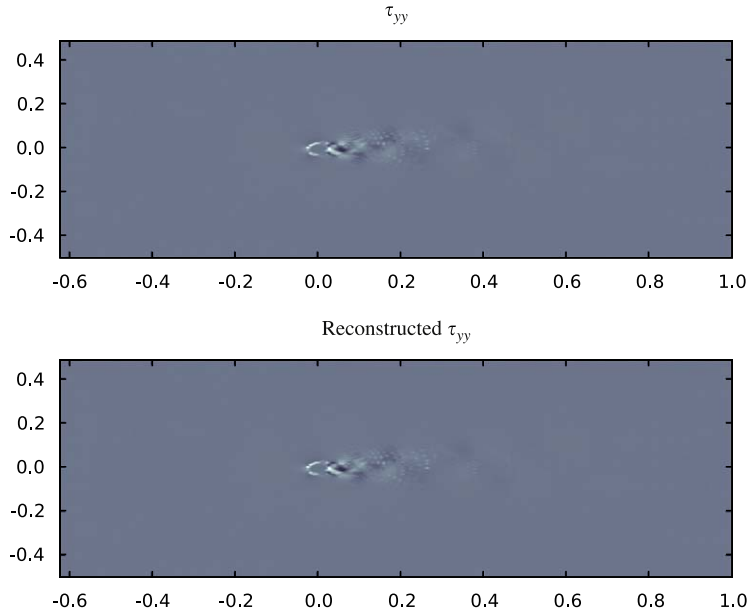


Fig. 13. Comparison of the 110th snapshot  $\tau_{yy}$  and those reconstructed.

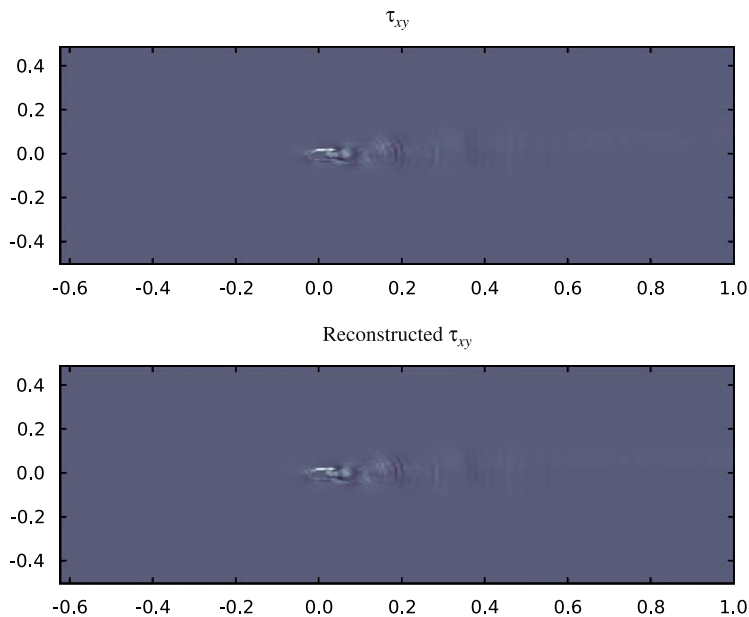


Fig. 14. Comparison of the 110th snapshot  $\tau_{xy}$  and those reconstructed.

The low-order dynamical system conserves the different properties of the flow. Another validation of the method consists in comparing the temporal coefficients.

Fig. 18 compares temporal coefficients obtained by the low-order dynamical system (36) and POD direct. The temporal coefficient  $a'_2$  is plotted versus  $a'_1$ .

If the low-order dynamical system is run for time period longer than the snapshot period, an outline circle is observed. This circle can be used to study the stability of the solution. The plot of  $a_2$  versus  $a_1$  has to approach the outline of this circle as much as possible.

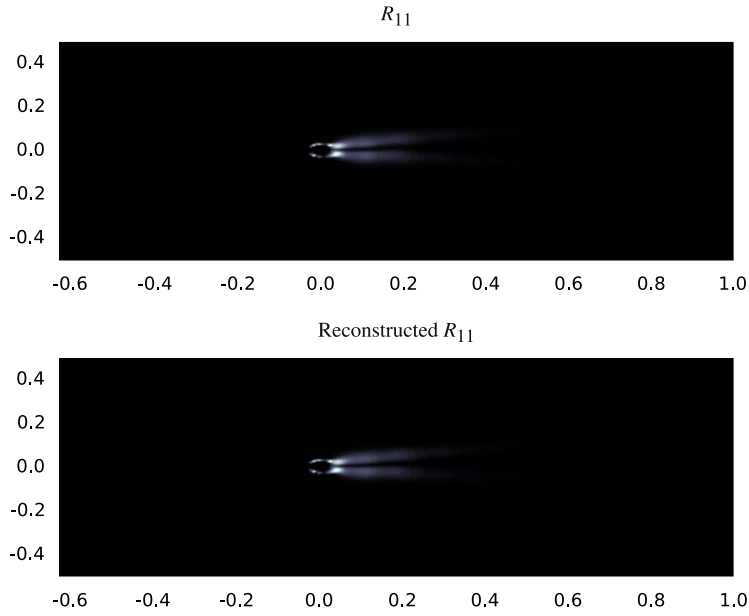


Fig. 15. Comparison of  $R_{11}$  and those reconstructed.

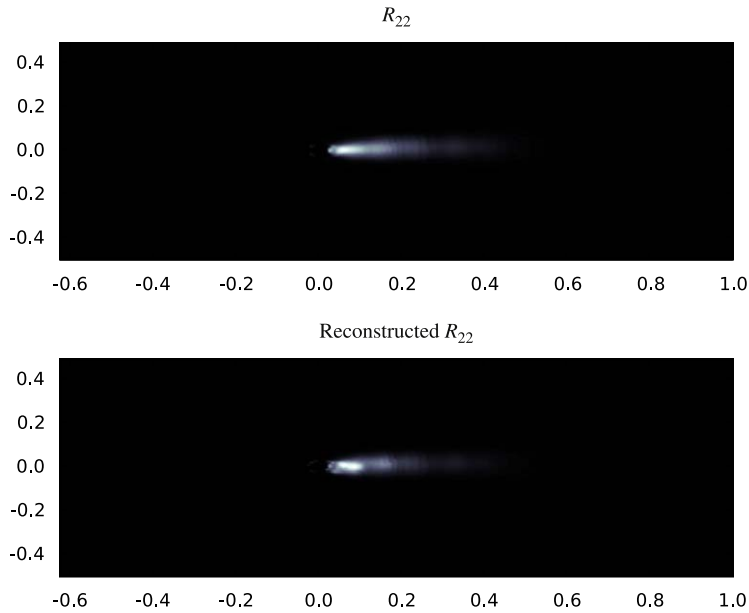
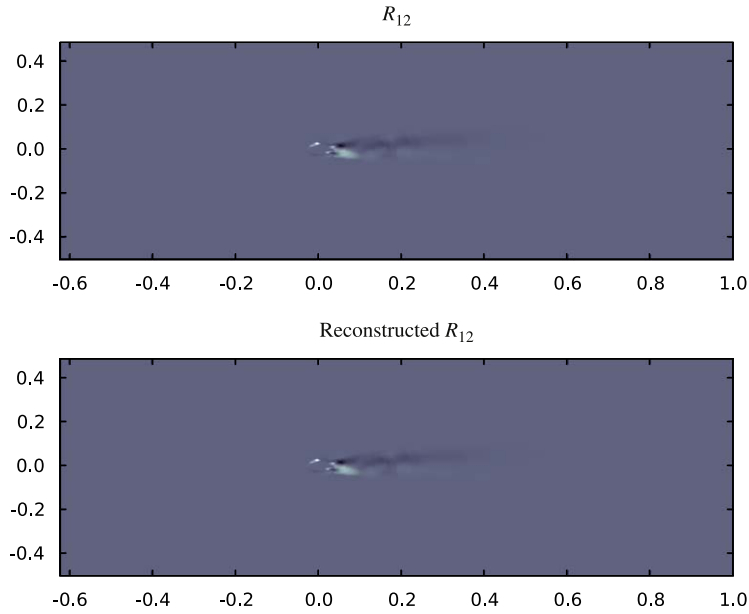
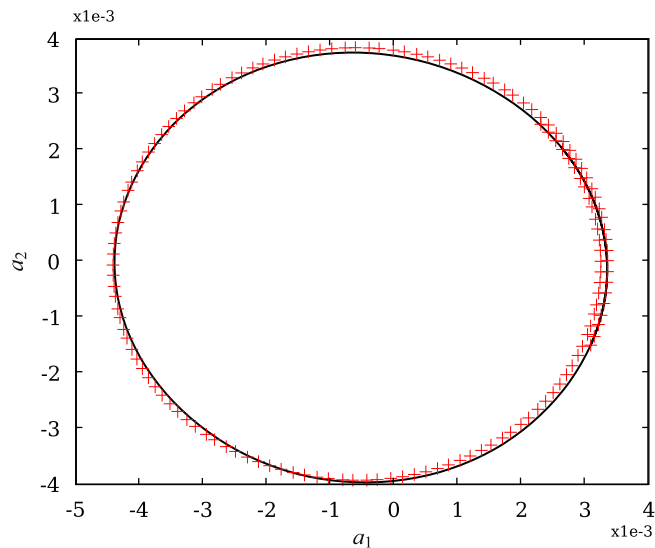


Fig. 16. Comparison of  $R_{22}$  and those reconstructed.

Fig. 19 plots the position of the gravity centre according to the  $x_2$  axis (the displacement has been blocked along  $x_1$ ). The result is also compared with the direct method which consists in projecting the discretised Navier–Stokes equations on the POD basis (Section 3.1). The same number of POD modes are considered for both, the direct method and the method proposed in this article. The result obtained by low-order dynamical system agrees with the results of the reference, however, the direct method does not give acceptable results.

Fig. 17. Comparison of  $R_{12}$  and those reconstructed.Fig. 18. Limit cycle  $a_2$  versus  $a_1$ : –, POD direct solution (41); +, obtained by ROM with 6 POD modes.

## 5. Conclusion

In this paper, the ROM method applied for fluid–structure interaction problem has been presented. The proper orthogonal decomposition (POD) method has been chosen due to its successful application to fluid mechanics problems. The main difficulty resides in the fact that the domain is moving, thus time-variant, while the POD basis has spatial properties. The proposed solution consists in computing the POD basis for the global velocity field (fluid and solid). Two methods for building ROM have been proposed. These methods used the fictitious domain approach and consist in extending the Navier–Stokes equations to the solid domain. The first method leads to a dynamical system whose coefficients have to be computed at each time step. In fact, a gain in terms of computational time is observed, but

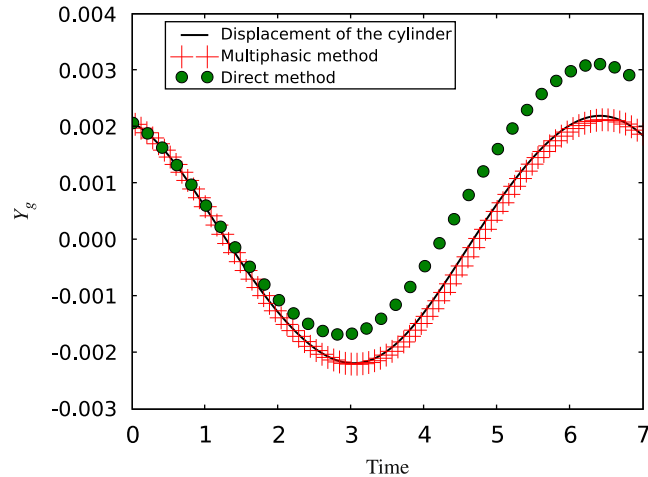


Fig. 19. Position of gravity centre: —, initial solution; +, obtained by our ROM method with 6 modes; •, obtained by the direct method with 6 modes.

the second solution leads to a better gain. The proposed approach has been validated by a test on a rigid cylinder oscillating in a fluid flow at a Reynolds number of 1690.

## References

- Abouri, D., Parry, A., Hamdouni, A., Longatte, E., 2006. A stable fluid–structure-interaction algorithm: application to industrial problems. *ASME Journal of Pressure Vessel Technology* 128 (4), 516–524.
- Allery, C., 2002. Contribution à l'identification des bifurcations et à l'étude des écoulements fluides par des systèmes d'ordre faible (pod). Ph.D. Thesis, Université de Poitiers, France.
- Allery, C., Bégheïn, C., Hamdouni, A., 2005. Applying proper orthogonal decomposition to the computation of particle dispersion in a two-dimensional ventilated cavity. *Communications in Nonlinear Science and Numerical Simulation* 10 (8), 907–920.
- Allery, C., Guerin, S., Hamdouni, A., Sakout, A., 2004. Experimental and numerical pod study of the Coanda effect used to reduce self-sustained tones. *Mechanics Research Communications* 31 (1), 105–120.
- Amabili, M., Sarkar, A., Padoussis, M.P., 2006. Chaotic vibrations of circular cylindrical shells: Galerkin versus reduced-order models via the proper orthogonal decomposition method. *Journal of Sound and Vibration* 290 (3–5), 736–762.
- Amabili, M., Touze, C., 2007. Reduced-order models for nonlinear vibrations of fluid-filled circular cylindrical shells: comparison of pod and asymptotic nonlinear normal modes methods. *Journal of Fluids and Structures* 23, 885–903.
- Anttonen, J.S.R., King, P.I., Beran, P.S., 2003. Pod-based reduced-order models with deforming grids. *Mathematical and Computer Modelling* 38 (1–2), 41–62.
- Anttonen, J.S.R., King, P.I., Beran, P.S., 2005. Applications of multi-pod to a pitching and plunging airfoil. *Mathematical and Computer Modelling* 42 (3–4), 245–259.
- Aubry, N., Guyonnet, R., Lima, R., 1991. Spatiotemporal analysis of complex signals: theory and applications. *Journal of Statistical Physics* 64 (3/4), 683–739.
- Aubry, N., Holmes, P., Lumley, J., Stone, E., 1988. The dynamics of coherent structures in the wall region of a turbulent boundary layer. *Journal of Fluid Mechanics* 192, 115–173.
- Baker, M.L., Mingori, D.L., Goggin, P.J., 1996. Approximate subspace iteration for constructing internally balanced reduced order models of unsteady aerodynamic systems. *AIAA Paper CP-1441*, 1070–1085.
- Berkooz, G., Holmes, P., Lumley, J.L., 1993. The proper orthogonal decomposition in the analysis of turbulent flows. *Annual Review of Fluid Mechanics* 25 (1), 539–575.
- Cazemier, W., Verstappen, R.W.C.P., Veldman, A.E.P., 1998. Proper orthogonal decomposition and low-dimensional models for driven cavity flows. *Physics of Fluids* 10 (7), 1685–1699.
- Couplet, M., 2005. Modélisation pod-Galerkin réduite pour le contrôle des écoulements instationnaires. Ph.D. Thesis, Université de Paris 13.
- Deane, A., Kevrekidis, I., Karniadakis, G., Orszag, S., 1991. Low-dimensional models for complex geometry flows—application to grooved channels and circular cylinders. *Physics of Fluids* 3, 2337–2354.
- Dowell, E.H., Hall, K.C., 2001. Modeling of fluid–structure interaction. *Annual Review of Fluid Mechanics* 33, 445–490.

- Glowinski, R., Pan, T., Hesla, T.I., Joseph, D.D., Periaux, J., 1999. A distributed lagrange multiplier/fictitious domain method for flows around moving rigid bodies: application to particulate flow. *International Journal for Numerical Methods in Fluids* 30 (8), 1043–1066.
- Hémon, P., Santi, F., 2003. Applications of biorthogonal decompositions in fluid–structure interactions. *Journal of Fluids and Structures* 17, 1123–1143.
- Holmes, P.J., Berkooz, G., Lumley, J.L., 1998. *Turbulence, Coherent Structures, Dynamical Systems and Symmetry*. Cambridge Monographs on Mechanics.
- Holmes, P.J., Lumley, J.L., Berkooz, G., Mattingly, J.C., Wittenberg, R.W., 1997. Low-dimensional models of coherent structures in turbulence. *Physics Report* 287 (4), 337–384.
- Karpel, M., 1982. Design for active flutter suppression and gust alleviation using state-space aeroelastic modelling. *Journal of Aircraft* 19 (3), 221–227.
- Liberge, E., 2008. Réduction de modèle par pod-Galerkin pour les problèmes d'interaction fluide structure (reduced order modeling by pod-Galerkin method in fluid-structure interaction). Ph.D. Thesis, La Rochelle University, France.
- Liberge, E., Benaouicha, M., Hamdouni, A., 2007. Proper orthogonal decomposition investigation in fluid structure interaction. *European Journal of Computational Mechanics* 16 (3–4), 401–418.
- Lieu, T., Farhat, C., Lesoinne, M., 2006. Reduced-order fluid/structure modeling of a complete aircraft configuration. *Computer Methods in Applied Mechanics and Engineering* 195 (41–43), 5730–5742.
- Longatte, E., Bendjeddou, Z., Souli, M., 2003. Methods for numerical study of tube bundle vibrations in cross-flows. *Journal of Fluids and Structures* 18 (5), 513–528.
- Longatte, E., Verreman, V., Souli, M., 2009. Time marching for simulation of fluid–structure interaction problems. *Journal of Fluids and Structures* 25 (1), 95–111.
- Lumley, J., 1967. The structure of inhomogeneous turbulent flows. In: Yaglom, A., Tararsky (Eds.), *Atmospheric Turbulence and Radio Wave Propagation*. Nauka Press, Moscow, pp. 166–178.
- Omurtag, A., Sirovich, L., 1999. On low-dimensional modeling of channel turbulence. *Theoretical and Computational Fluid Dynamics* 13, 115–127.
- Patankar, N., Singh, P., Joseph, D., Glowinski, R., Pan, T.-W., 2000. A new formulation of the distributed lagrange multiplier/fictitious domain method for particulate flows. *International Journal of Multiphase Flows* 26, 1509–1524.
- Perrin, R., Braza, M., Cid, E., Cazin, S., Sevrain, A., Strelets, M., Shur, M., Hoarau, Y., Barthet, A., Harran, G., Moradei, F., 2006. 3d circular cylinder. *Notes on Numerical Fluid Mechanics* 94, 299–312.
- Peskin, C.S., 1973. Flow patterns around heart valves: a digital computer method for solving the equations of motion. *IEEE Transactions on Biomedical Engineering BME-20* (4), 316–317.
- Rempfer, D., 1996. Investigations of boundary layer transition via Galerkin projections on empirical eigenfunctions. *Physics of Fluids* 8, 175–188.
- Rempfer, D., Fasel, H.F., 1994. Evolution of three-dimensional coherent structures in a transitional flat-plate boundary layer. *Journal of Fluid Mechanics* 275, 257–283.
- Romanowski, M., Dowell, E., 1996. Reduced order euler equation for unsteady aerodynamics flow: numerical techniques. *AIAA Paper* 96-0528.
- Sirovich, L., 1987. Turbulence and the dynamics of coherent structures, part i: coherent structures; part ii: symmetries and transformations; part iii: dynamics and scaling. *Quarterly of Applied Mathematics* 45 (3), 561–590.
- Sirovich, L., Ball, K., Keefe, L., 1990. Planes waves and structure in turbulent channel flow. *Physics of Fluids A2* 12, 2217–2226.
- Trindade, M.A., Wolter, C., Sampaio, R., 2005. Karhunen-Loève decomposition of coupled axial/bending vibrations of beams subject to impacts. *Journal of Sound and Vibration* 279 (3–5), 1015–1036.
- Utturkar, Y., Zhang, B., Shyy, W., 2005. Reduced-order description of fluid flow with moving boundaries by proper orthogonal decomposition. *International Journal of Heat and Fluid Flow* 26 (2), 276–288.